J Solid State Electrochem (2011) 15:405–412
DOI 10.1007/s10008-010-1102-0

ORIGINAL PAPER

Effect of calcium hydroxide on the electrochemical performance of a $[Ni_4Al(OH)_{10}]OH$ electrode

Liwei Qin · Meng Hu · Xiaorui Gao · Lixu Lei

Received: 8 May 2009 / Revised: 10 May 2010 / Accepted: 11 May 2010 / Published online: 25 May 2010

Abstract Samples of $[Ni_4Al(OH)_{10}]OH$ were prepared by co-precipitation with the existence of calcium and subsequent hydrothermal treatment. Inductively coupled plasma (ICP) measurements show that the composition of prepared samples does not change very much with the initial concentration of Ca^{2+} in the mother solution, which may be related to the high solubility of $Ca(OH)_2$. Powder X-ray diffraction measurements show that the modification does not change the lattice parameters of $[Ni_4Al(OH)_{10}]OH$ a lot, but scanning electron microscope images show some morphological differences between the sample without Ca and the sample after the modification of calcium hydroxide. However, those changes in composition and morphology do improve the reversibility and charge efficiency of $[Ni_4Al(OH)_{10}]OH$, especially at a higher temperature of 65 °C. For example, the difference between the oxidation peak and oxygen evolution peak in the cyclic voltammetric diagrams at 65 °C becomes large, a better charge/discharge performance at high current density can be observed. In addition, the charge-transfer resistance (R_t) of the electrode according to the electrochemical impedance spectra increases after the modification of calcium and become larger as the temperature is elevated for 20 to 65 °C.

Keywords $[Ni_4Al(OH)_{10}]OH$ · Calcium modification · High temperature · Current density · Charge-transfer resistance

L. Qin · M. Hu · X. Gao · L. Lei (✉)
School of Chemistry and Chemical Engineering,
Southeast University,
Nanjing 211189, China
e-mail: lixu.lei@seu.edu.cn

Introduction

Up to now, commercial nickel-metal hydride (Ni-MH) batteries still employ metal hydrides and β-$Ni(OH)_2$ as negative and positive electrode materials, respectively. They are safer and faster in chargeability than lithium-ion batteries, yet present high energy and power density, excellent long-term cycling stability [1–3], therefore, Ni-MH batteries are regarded as a good choice for electric vehicles. When β-$Ni(OH)_2$ is charged, it transforms into β-NiOOH and releases one electron, therefore it has a maximum capacity of 289 $mAh \cdot g^{-1}$. β-$Ni(OH)_2$ has a shortcoming, that is when the batteries are overcharged or float-charged for a long period of time, γ-NiOOH appears, which results in a serious expansion and consequent mechanical deformation of the electrode, and thus impairs the electrode performances. However, it is difficult to limit the overcharge for uses in electric vehicles.

On the contrary, the transformation of α-$Ni(OH)_2$ to γ-NiOOH causes a small contraction and therefore only a little mechanical deformation. The transformation usually produces more than one electron since the oxidation state of nickel in γ-NiOOH could be as high as 3.7 [4, 5], which leads to a much higher theoretical capacity than β-$Ni(OH)_2$. However, there are two problems with the couple of α-$Ni(OH)_2$ and γ-NiOOH: one is that pure α-$Ni(OH)_2$ is very unstable in strong alkaline medium and easily transforms into the β-$Ni(OH)_2$ after a few electrochemical cycles; another is that the density of α-$Ni(OH)_2$ is lower, which leads to smaller volumetric specific capacity than β-$Ni(OH)_2$.

It has been found that partial substitution of other cations such as Co [6], Al [7–10], Fe [11], Mn [12], and Zn [13] for Ni can increase the stability of α-$Ni(OH)_2$ in strong alkaline media. Among these metal elements, Al is the most

attractive one because of its high stability in trivalent state and cheapness. Studies show that Al stabilized α-$Ni(OH)_2$ has much higher gravimetric capacity, longer cycle life than β-$Ni(OH)_2$, consequently, they are nominated as the electrode material for light weight Ni-MH batteries [7, 14, 15].

Recently, we have found that a layered double hydroxide (LDH), $[Ni_4Al(OH)_{10}]OH$ can be charged and discharged at very high current densities and yet it has a long cycle life; the material is also not sensitive to overcharging, therefore, it is very attractive for batteries of heavy-duty purposes [8–10]. To make it be used in commercial batteries, we have reported the effects of Zn doping on the electrochemical performance of $[Ni_4Al(OH)_{10}]OH$ [16].

When batteries are used as power source for electric and hybrid electric vehicles, they are usually required to work in an environment from −20 °C to over 40 °C. Therefore, performances under low and high temperature of Ni-MH batteries have been received much attention from both industry and research labs. It is known that charge efficiency and discharge capacity can be seriously affected at high temperatures [17, 18].

Oxygen evolution is a factor that declines charge efficiency of positive electrodes, and it simply depends on the positive electrode at elevated temperature (>50 °C). Studies showed that addition of cobalt or cobalt compounds [19, 20], ZnO [21], CdO [22], lanthanide oxides [22, 23] and calcium compounds [24–27] can improve the high-temperature electrochemical performance of β-$Ni(OH)_2$ electrodes, because they can improve the utilization, charge-discharge reversibility, increase the oxygen evolution potential, and suppress γ-NiOOH formation of the electrode materials. As it is known that those additives may act differently for different electrodes, we would like to see how they act to our $[Ni_4Al(OH)_{10}]OH$.

Among the additives listed above, cobalt and lanthanide are expensive; and cadmium is very toxic, therefore, we chose calcium to study its effect on the high-temperature performance of $[Ni_4Al(OH)_{10}]OH$.

Experimental

Preparation of $[Ni_4Al(OH)_{10}]OH$ samples with different contents of calcium

The samples were prepared by a similar method to our previous paper [9]. Under protection of N_2 flow and vigorous stirring, an aqueous solution of sodium hydroxide (0.25 mol·l^{-1}) was slowly dropped into a solution of 5.00 g $Ni(NO_3)_2{\cdot}6H_2O$, 1.62 g $Al(NO_3)_3{\cdot}9H_2O$ and some Ca $(NO_3)_2{\cdot}4H_2O$ in 100 ml distilled water at 100 °C in an hour, and the final pH value of the solution is about 8.0. After the reaction mixture was stirred for another 18 h, it was transferred into several hydrothermal vessels, which were maintained at 180 °C for 24 h. The solid product was then filtered out, washed with water, and then undergone ion exchange at 20 °C for 10 h using aqueous solution of sodium hydroxide (0.25 mol·l^{-1}). Finally, it was filtrated, washed and dried in vacuum at 80 °C.

Four samples were prepared in the mother solution in this study. The sample without the adding of Ca $(NO_3)_2{\cdot}4H_2O$ was denoted as sample 1; and the samples with the adding of 0.76 g; 1.02 g; 0.50 g $Ca(NO_3)_2{\cdot}4H_2O$ in the starting solution were denoted as samples 2, 3, and 4, respectively.

Materials characterization

Elemental analysis of nickel, aluminum, and calcium was performed by analytical service of Nanjing University by using a Jarrel-Ash J-A1100 ICP spectrophotometer. Powder X-ray diffractograms were recorded on a Rigaku D/MAX 2200 diffractometer using Cu Kα radiation (λ=1.54056 Å). Scanning electron microscopy (SEM) was performed on a JEOL JSM-561-LV scanning electron microscope.

Preparation of electrodes

Preparation of the electrodes: 50 mg of as prepared sample, 160 mg of Ni powder, 40 mg of Co powder and several drops of 5 wt.% aqueous polytetrafluoroethylene suspension were mixed thoroughly to obtain a paste in an agate mortar. A piece of nickel foam sized φ15 mm was sandwiched with the paste using a spatula, dried at 80 °C for 24 h, then pressed at 20 MPa for 1 min to assure good electrical contact between the substrate and the active material. The electrode had been immersed in 7 mol·l^{-1} potassium hydroxide (KOH) solution for 24 h before usage.

Electrochemical tests

Electrochemical tests were performed in a three-compartment electrolysis cell. A piece of nickel foam was employed as the counter electrode, Hg/HgO electrode in 7 mol·l^{-1} KOH solution as the reference electrode. Here, the concentration of KOH solution was 7 mol·l^{-1} because Ni-MH batteries usually employ 6~7 mol·l^{-1} KOH solution [10, 16]. Charge/discharge cycling performances were conducted using a LAND CA2001A cell performance-testing instrument (Wuhan, China). The working electrode was charged at a constant current density of 100 mA·g^{-1} for 4 h, and then discharged at the same current density until the potential decreases to 0 V (vs. Hg/HgO in 7 mol·l^{-1} KOH aqueous solution). After five cycles, the electrode

Table 1 Chemical composition of the prepared samples

Sample	Stoichiometric formula	Elemental analysis	
		Observed	Calculated
1	$[Ni_{3.92}Al\ (OH)_{9.84}]OH{\cdot}7.0\ H_2O$	Ca 0; Ni 40.40; Al 4.74	Ca 0; Ni 40.54; Al 4.75
2	$[Ni_{3.93}Al(OH)_{9.86}]OH{\cdot}0.08Ca(OH)_2{\cdot}6.7H_2O$	Ca 0.58; Ni 40.60; Al 4.75	Ca 0.56; Ni 40.54; Al 4.74
3	$[Ni_{4.02}Al(OH)_{10.04}]OH{\cdot}0.09Ca(OH)_2{\cdot}6.4H_2O$	Ca 0.66; Ni 41.40; Al 4.74	Ca 0.63; Ni 41.20; Al 4.71
4	$[Ni_{4.03}Al(OH)_{10.06}]OH{\cdot}0.07Ca(OH)_2{\cdot}6.0H_2O$	Ca 0.52; Ni 41.90; Al 4.69	Ca 0.50; Ni 41.88; Al 4.69

was charged at 800 $mA{\cdot}g^{-1}$ for 30 min and discharge at 400 $mA{\cdot}g^{-1}$ to 0 V.

Cyclic voltammetry diagrams were measured after 20 charge/discharging cycles by a CHI660b (Shanghai, China) electrochemical workstation at a scan rate of 0.1 $mV{\cdot}s^{-1}$ from 0.10 to 0.70 V. Electrochemical impedance spectroscopy (EIS) data were measured under open circuit with a frequency range from 100 kHz to 50 mHz, the number of points per decade is twelve and the wave amplitude is 5 mV (peak-to-peak). Experimental data of the impedance plot were analyzed by applying the nonlinear least squares fitting to the appropriated theoretical model represented by an equivalent electrical circuit.

Results and discussion

Chemical composition, structure and morphology of the samples

Ni, Al, or Ca in the four samples were analyzed by ICP and the results are shown in Table 1. It shows molar ratios of nickel to aluminum are all around 4.0, which are consistent with the initial ratio of the starting materials employed in the preparation of materials. However, the molar ratios of calcium to aluminum are all less than 0.1 and remain about the same in the samples containing calcium, which are very different from the molar ratio in the mother solution. The reason may be that $Ca(OH)_2$ was washed away by the subsequent washing during the preparation of materials, because $Ca(OH)_2$ is relatively highly soluble in water. According to the solubility product of $Ca(OH)_2$, which is 5.5×10^{-6}, the solubility is about 0.011 $mol{\cdot}l^{-1}$, which means that all the Ca^{2+} in $Ca(OH)_2$ can dissolve in 400 ml H_2O for the sample 4.

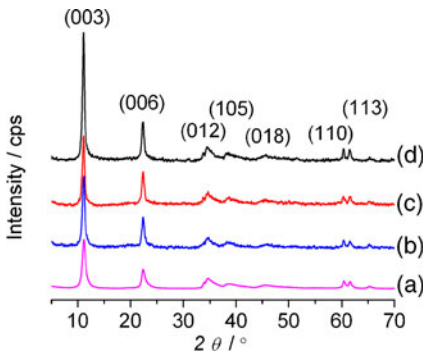

Fig. 1 XRD patterns of **a** sample 1 (without calcium) and **b** sample 2 (0.58 wt.% Ca); **c** sample 3 (0.66 wt.% Ca) and **d** sample 4 (0.52 wt.% Ca)

Figure 1 shows the X-ray diffraction (XRD) patterns of the prepared samples with different contents of calcium. It is obvious that all of them share great similarities. All the diffraction peaks can be indexed on a hexagonal cell, space group *P*6222, and the parameters for sample 1 (without calcium) (a=3.060 Å, c=23.75 Å) almost have little difference from the samples containing calcium (a= 3.063 Å, c=23.96 Å). In addition, there are not any diffraction peaks of calcium hydroxide (JCPDS 84–1,270) in the XRD patterns. Ca^{2+} (99 pm) is much bigger than Ni^{2+} (69 pm) and Al^{3+} (54 pm), therefore, the fact that calcium modification does not change the crystal structure and the lattice parameters of $[Ni_4Al(OH)_{10}]OH$ very much may mean that Ca^{2+} seldom replace Ni^{2+} or Al^{3+} in the lattice, but $Ca(OH)_2$ may amorphously cover the grains. We also noticed that the particle size of each sample containing calcium is larger than sample 1 (without calcium), i.e., $[Ni_4Al(OH)_{10}]OH$ shown in Table 2, indicating Ca^{2+} or $Ca(OH)_2$ may have some effects on the growth of crystals for the materials.

The SEM images of sample 1 (without Ca) and sample 2 (0.58% Ca) are illustrated in Fig. 2, in which aggregated flaky crystals are seen in both samples. The flakes are a few micrometers in size in both samples, but sample 2 seems have irregular edges like gear wheels.

Table 2 The obtained XRD data of the samples and their calculated particle sizes

Sample	2θ of (003) reflection (°)	*FWHM* (°)	*d* Value (nm)	Particle size (nm)
1	11.17	0.746	0.791	10.0
2	11.06	0.490	0.799	15.2
3	11.09	0.540	0.797	13.8
4	11.07	0.444	0.799	16.7

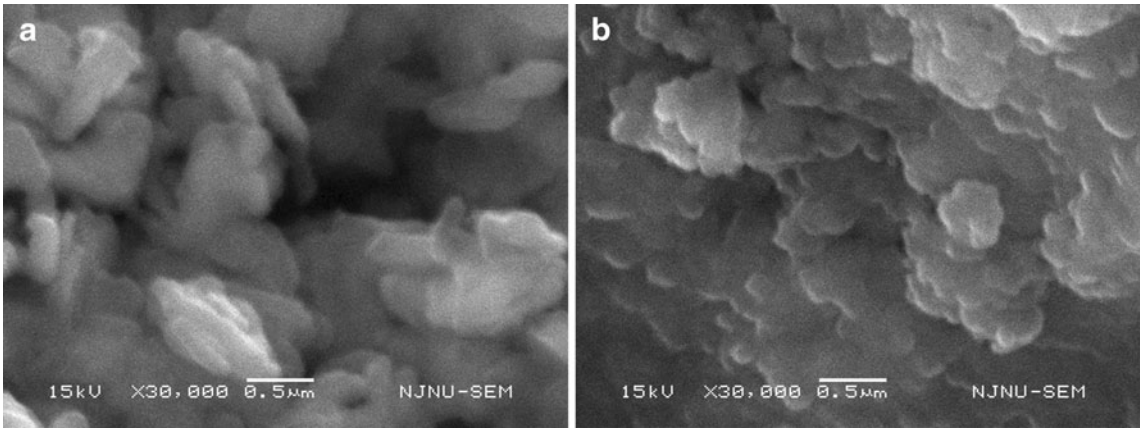

Fig. 2 SEM images of **a** sample 1 (without Ca) and **b** sample 2 (0.58% Ca)

In summary, it can be concluded that the samples are LDHs of a Ni/Al ratio of approximate 4:1, the interlayer anion is OH^- and there is a little $Ca(OH)_2$ which may cover the surface of the LDH particles. The existing of $Ca(OH)_2$ during the preparation causes the morphological changes of the disk-like LDH particles, which looks like gear wheels, but other structural characters do not changes very much.

Electrochemical behaviors

Figure 3 shows the cyclic voltammogram curves of sample 1 (without Ca) and sample 2 (0.58% Ca) after 20 charge-discharge cycles at indicated temperature. Table 3 gives the information about characteristic potential values of such cyclic voltammetric results.

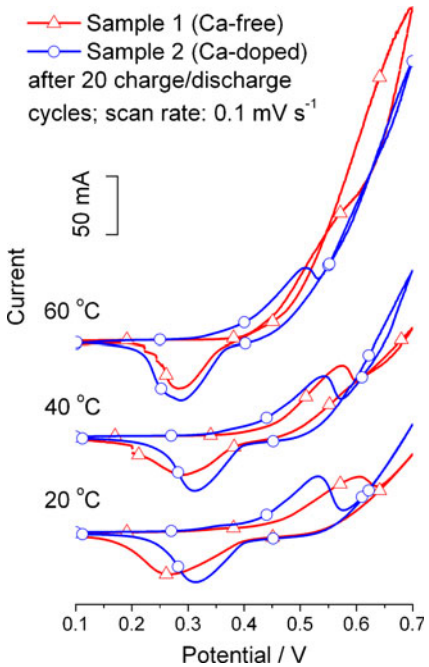

Fig. 3 Cyclic voltammetric curves of sample 1 (without Ca) and sample 2 (0.58 wt.% Ca) at the temperature of 20 °C, 40 °C, and 65 °C at a scan rate of 0.1 mV s^{-1} after 20 charge/discharging cycles

It can be seen from Fig. 3 and Table 3 that the reductive potentials for each sample remain about the same, but the oxidative potentials and oxygen evolution potentials change a lot as the temperature rises. It seems that calcium modification can lower ΔE_{ac} and E_{pc} values, thus decrease the tendency of oxygen evolution as higher temperatures (Fig. 3). We are especially interested in the difference between the oxidative potential and oxygen evolution potentials, because it has significant effect on the charge efficiency of the electrode. There is no oxidation peak for sample 1 at 65 °C, which means that the $[Ni_4Al(OH)_{10}]OH$ electrode cannot be charged efficiently since the evolution of oxygen cannot be avoided. This is in accordance with the literature [28]. However, that case can be change since the difference between oxidation of the electrode and oxidation of water still exists distinguishably at 65 °C for sample 2, and it is more distinguishable at each experimental temperature than sample 1. This may be understood as it was suggested that evolution of oxygen can occur at surface of NiOOH, and metal cations with s^2p^6 electron configuration (such as Ca^{2+} and Y^{3+}) can react with NiOOH, leading to the inhibition of the electron transfer and the increase of the oxygen evolution potential [29, 30]

Table 3 Potential value of voltammetric features for Samples 1 and 2 at different temperatures

Temperature	Sample 1 (without Ca)			Sample 2 (0.58% Ca)		
	E_{pc}(V)	E_{pa}(V)	ΔE_{ac}(V)	E_{pc}(V)	E_{pa}(V)	ΔE_{ac}(V)
20 °C	0.621	0.264	0.357	0.531	0.313	0.218
40 °C	0.576	0.285	0.291	0.544	0.312	0.232
65 °C	–	0.282	–	0.570	0.289	0.281

Note: E_{pc} is the oxidative potential; E_{pa} is the reductive potential and ΔE_{ac} is the difference between E_{pc} and E_{pa}

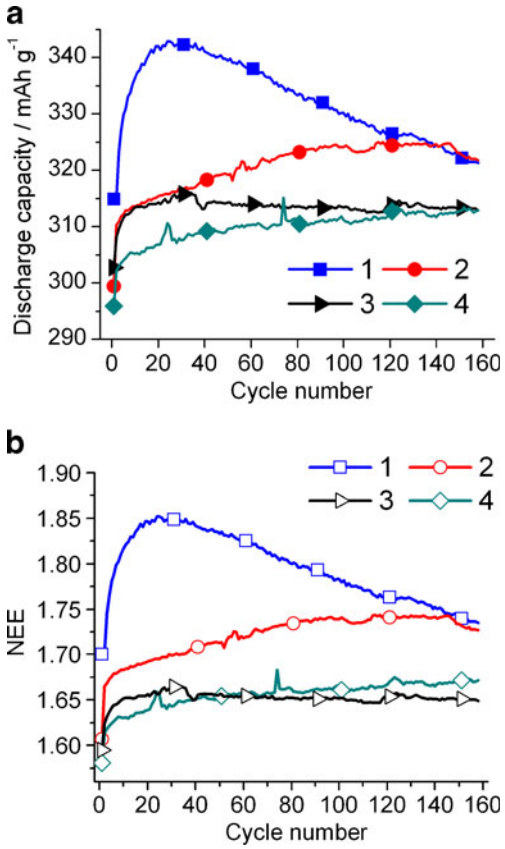

Fig. 4 Variations of (**a**) discharge capacity and (**b**) the number of exchanged electrons per nickel atom (*NEE*) to the cycle number at 20 °C. The curves denoted with 1, 2, 3, and 4 are sample 1 (without Ca), Sample 2 (0.58 wt.% Ca), sample 3 (0.66 wt.% Ca) and sample 4 (0.52 wt.% Ca), respectively. The electrodes were charged at a constant current density of 100 mA·g^{-1} for 4 h, and then discharged at the same current density until the potential decreases to 0 V (vs. Hg/HgO in 7 mol·l^{-1} KOH aqueous solution). After five cycles, the electrode was charged at 800 mA·g^{-1} for 30 min and discharge at 400 mA·g^{-1} to 0 V

Figure 4a shows variations of the specific discharging capacity to the cycle number. It is obvious that the capacity of sample 1 is higher than the other samples at 20 °C, but the samples modified by calcium hydroxide exhibit a better cyclic stability. For example, the capacity of sample 2 (with 0.58 wt.% Ca) can maintain at 320 mAh·g^{-1} after 160 cycles, while that of sample 1 (without Ca) decreased rapidly from 343 mAh·g^{-1} to less than 320 mAh·g^{-1} after the same cycles. The cyclic stabilities for the samples with calcium are basically similar, but they do have some difference. This may be related to the particle size [8], composition, and morphology. Tables 1 and 2 show the difference of the samples in composition and size. Figure 4b also shows the corresponding variations of the number exchanged electrons per nickel atom (NEE) to the cycle number. Obviously, calcium modification lowers the NEE, therefore, lowers the discharging capacity of the active materials.

Figure 5a shows variations of the specific discharging capacity to the cycle number at different temperatures. The discharging capacities of samples 1 and 2 become smaller as the temperature rises from 20 °C to 40 °C, but it is very interesting that the discharge capacities at 65 °C decrease after about 20 cycles and then begin to increase after 40 cycles again. This decrease may be attributed to the structural transformation of the active materials, e.g. layered double hydroxides to β-Ni(OH)$_2$ at the high temperature of 60 °C (the details of such transformation have been observed and will be further studied). The subsequent increase may come from the oxidation of nickel in the conducting agent, which slowly transforms into nickel hydroxide as the cycle number goes and forms some discharge capacity. This was confirmed by the following experiment.

Figure 6 shows variations of the specific discharging capacity to the cycle number with graphite as the conductive additive, compared to those with the mixture of nickel and cobalt powder. Clearly the discharge capacity decreases and stabilizes later as cycle number increases when graphite as the conductive additive, which is in contrast to that when Ni and Co powders are used.

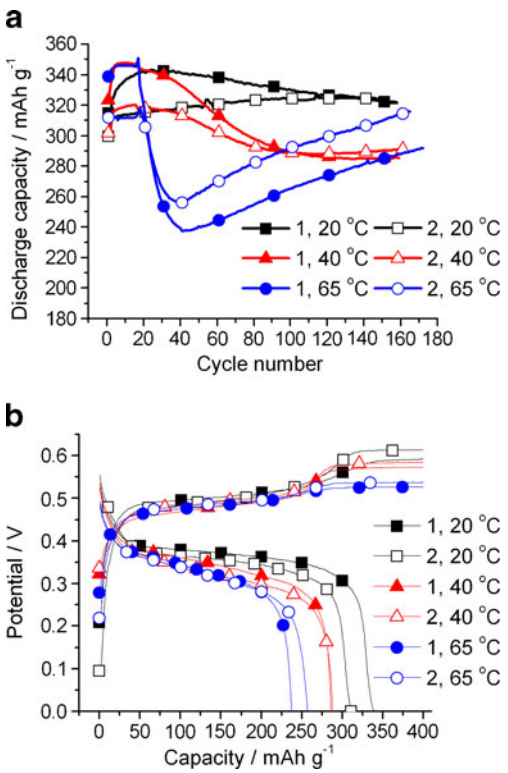

Fig. 5 **a** Variations of the specific discharging capacity at different temperatures to the cycle number, **b** charge-discharge curves of sample 1 (without Ca) and sample 2 (0.58 wt.% Ca). The electrodes were charged at a constant current density of 100 mA·g^{-1} for 4 h, and then discharged at the same current density until the potential decreases to 0 V. After five cycles, the electrode was charged at 800 mA·g^{-1} for 30 min and discharge at 400 mA·g^{-1} to 0 V

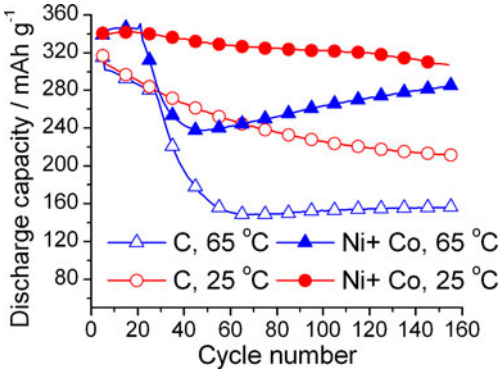

Fig. 6 The cycle life of the $[Ni_4Al(OH)_{10}]OH$ electrode with graphite and a mixture of nickel and cobalt powder as the conducting agent at the indicated temperatures

Figure 5b shows that the discharge potentials decrease while charge potentials do not change very much with the increase of temperature, and calcium modification (sample 2) lowers the discharge potentials in each circumstance.

Electrochemical impedance spectroscopy measurements

The EIS of sample 1 (without Ca) and 2 (0.58 wt.% Ca) electrodes were measured at the 100% depth of discharge (DOD). Figure 7a–c show the Nyquist plots of samples 1 and 2 electrodes at three different temperatures. Each Nyquist plot comprises a depressed semicircle at high frequency and a straight line at lower frequency. At a lower temperature such as 20 °C, a much smaller semicircle is observed for both samples 1 and 2, and the electrode is mainly controlled by a diffusion process as reported by us [10]. As the temperature is elevated, the semicircle becomes bigger which means that the electron transfer impedance, R_t increases. Thus, the electrode controlled by diffusion becomes an electrode controlled by a combination of kinetics and diffusion. It is believed that the diffusion is weakened by the rapidly moving ions at higher temperatures and the role of electron transfer in the redox reaction stands out.

Figure 7d shows the equivalent circuit used to analyze experimental results. Table 4 lists the fitted electrochemical parameters according to the equivalent circuit. It is obvious that the solution resistance, R_s for both samples are similar, although that of sample 2 (with calcium) is always bigger than that of sample 1 (without Ca) shown at each temperature. It is agreed that R_s changes with the composition of nickel hydroxide layers [31, 32] and the DOD [32], therefore existence of calcium could lead to 12the difference. The Q_c is related to double electric layer which depends on the angular frequency, ω as well as the adjustable parameters *n,* which can be understood as a measure of microscopic irregularities and has a value between 0.5 (porous electrodes) and unity (ideally flat electrodes). Therefore, Q_c may be affected by surface

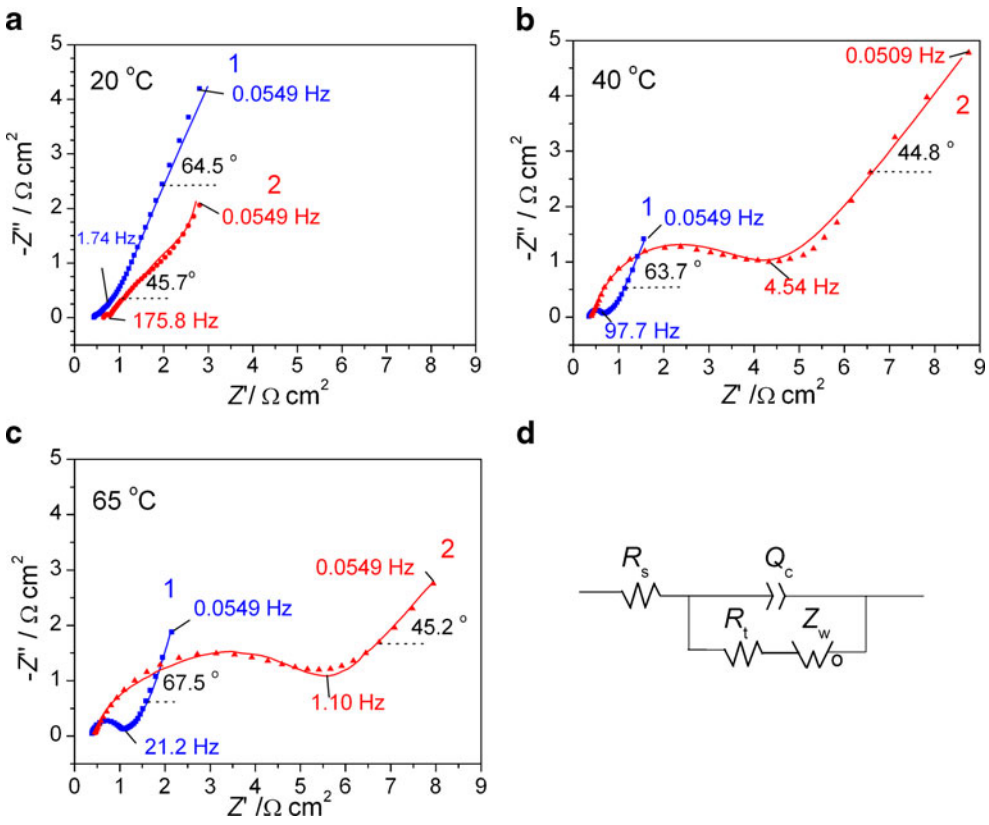

Fig. 7 Nyquist plots of sample 1 (without Ca) and sample 2 (0.58 wt.% Ca) electrodes at **a** 20 °C; **b** 40 °C; **c** 65 °C; and **d** an equivalent circuit. The *solid lines* represent the best fit to the circuit diagram

Table 4 The EIS fitting results of Samples 1 (without Ca) and 2 (0.58 wt.% Ca)

Temperature/°C	Sample	R_s/Ω·cm^2	R_t/Ω·cm^2	Q_c/F cm^2		Z_w/Ω·cm^2		
				Y_1	n_1	R_0	Y_2	n_2
20	1	0.43	0.014	0.0016	1.0	0.68	0.15	0.33
	2	0.65	0.094	0.00050	1.0	6.29	11.31	0.47
40	1	0.36	0.24	0.00053	0.98	0.88	1.26	0.35
	2	0.42	2.60	0.0018	0.82	4.63	1.68	0.27
65	1	0.37	0.61	0.0010	0.88	1.07	1.21	0.37
	2	0.43	3.86	0.0056	0.71	5.00	5.83	0.27

Notes: R_s is the total ohmic resistance of the solution; Q_c is a constant phase element capacity; R_t is the charge-transfer resistance of the electrodes which is related to the ionic transportation; Z_w is the Generalized Finite Warburg impedance of the solid phase diffusion. The impedance of Q_c can be described as: $Q_c = \frac{1}{Y(i\omega)^n}$, where Y is the admittance, ω is the angular frequency in rad·s^{-1} and the value of n=1 corresponds to capacitance, n=0 corresponds to resistance and n=0.5 corresponds to Warburg diffusion. The Warburg impedance, Z_w can be described as $Z_W = R_0 \frac{\mathrm{ctnh}(iY\omega)^n}{(iY\omega)^n}$ [33, 35], where Y, n are adjustable parameters, $Y=L^2/D$, L is the effective diffusion thickness and D is the effective diffusion coefficient of the particle, R_0 is a parameter related to L, D, and R_t

roughness of solid electrodes [33, 34]. From this view of point, it seems that the electrodes become more porous as temperature goes higher. From a new observation on the electrode, we know that higher temperature could cause the loss of aluminum easier, which causes cracks and unstablility of $[Ni_4Al(OH)_{10}]OH$. We thought that similar thing happens here.

We are more interested in the electron transfer resistance, R_t which relates to the electrochemical reactions. As shown in Fig. 8, the plots of R_t against the temperature clearly indicate that there are great differences between the two samples. According to the analyses in the previous part of the paper, $Ca(OH)_2$ or Ca^{2+} may cover the surface of the material grains. However, they are electrochemical inactive and cannot be involved in the redox reaction. Therefore, they may be thought as obstacles, jamming the passages for ion transfers and reducing the contact surface for the electrochemical reaction. These result in a little worse cycling performance for sample 2 as shown in Fig. 4. The linear part due to the Warburg diffusion for samples 1 and 2 has a slope of about 65° and 45°, respectively; and the slope seems to have no much large variations as the temperature is elevated. The slope can be seen as an empirical parameter related qualitatively to the Warburg diffusion resistance where a higher slope signifies a slower rate of diffusion, and a low slope a more rapid rate of diffusion [36, 37].

On the other hand, these obstacles can protect the surface of the material from corrosion from the highly concentrated alkali solution (7 mol·l^{-1} KOH) because an observation shows that the LDH material can transform into β-$Ni(OH)_2$ after Al^{3+} ions leave the hydroxide layers especially at a higher temperature of 60 °C (to be published by us). Therefore, in the long-time charge/discharge cycles the increase of electron transfer resistance by the introduction of calcium can be trade off the electrode performance, especially its high-temperature performance.

Conclusions

Calcium hydroxide modified $[Ni_4Al(OH)_{10}]OH$ was co-precipitated at 100 °C and then hydrothermally treated at 180 °C for 24 h. It was found that the content of Ca^{2+} remains almost the same in spite that the concentration of Ca^{2+} in the mother solution is different. That is probably related to the high solubility of $Ca(OH)_2$. The calcium modification does not change the lattice parameters of $[Ni_4Al(OH)_{10}]OH$ a lot, yet it changes its morphology and electrochemical performance: (1) the NEE per Ni atom is lowered; (2) the difference between the oxygen evolution potential and the oxidative potential of $[Ni_4Al(OH)_{10}]OH$ enlarged, especially at 65 °C; (3) cyclic stability of electrode can be improved by the calcium modification; (4) according to the analysis of EIS, the charge-transfer

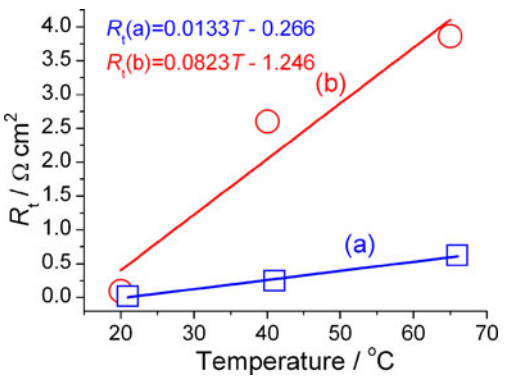

Fig. 8 The plots of R_t against the temperature: **a** sample 1 (without Ca) and **b** sample 2 (0.58 wt.% Ca)

resistance of the electrode at higher temperatures increases more significantly than the sample without calcium.

References

1. Ovshinsky SR, Fetcenko MA, Ross J (1993) Science 260:176
2. Linden D (1995) Handbook of batteries. McGraw-Hill, New York
3. Fetcenko MA, Ovshinsky SR, Reichman B, Young K, Fierro C, Koch J, Zallen A, Mays W, Ouchi T (2007) J Power Sources 165:544
4. Barnard R, Randell CF, Tye FL (1980) J Appl Electrochem 10:127
5. Corrigan DA (1989) J Electrochem Soc 136:7
6. Faure C, Delmas C, Willmann P (1991) J Power Sources 36:497
7. Hu WK, Noreus D (2003) Chem Mater 15:974
8. Hu M, Lei L (2007) J Solid State Electrochem 11:847
9. Lei L, Hu M, Gao X, Sun Y (2008) Electrochimica Acta 54:671
10. Hu M, Gao X, Lei L, Sun Y (2009) J Phys Chem C 113:7448
11. Guerlou-Demourgues L, Fournes L, Delmas C (1996) J Electrochem Soc 143:3083
12. Wu MY, Wang JM, Zhang JQ, Cao CN (2006) J Solid State Electrochem 10:411
13. Chen H, Wang JM, Zhao YL, Zhang JQ, Cao CN (2005) J Solid State Electrochem 9:421
14. Kamath PV, Dixit M, Indira L, Shukla AK, Kumar VG, Munichandraiah N (1994) J Electrochem Soc 141:2956
15. Wang CY, Zhong S, Bradhurst DH, Liu HK, Dou SX (2002) J Alloy Compd 330–332:802
16. Gao X, Lei L, Hu M, Qin L, Sun Y (2009) J Power Sources 191:662
17. Shinyama K, Magari Y, Funahashi A, Tanaka K (2003) Electrochemistry 71:686
18. Hu WK, Gao XP, Geng MM, Gong ZX, Noreus D (2005) J Phys Chem B 109:5392
19. Watanabe K, Koseki M, Kumagai N (1996) J Power Sources 58:23
20. Pralong V, Delahaye-Vidal A, Beaudoin B, Leriche JB, Tarascon JM (2000) J Electrochem Soc 147:1306
21. Tessier C, Faure C, Guerlou-Demourgues L, Denage C, Nabias G, Delmas C (2002) J Electrochem Soc 149:A1136
22. Oshitani M, Watada M, Shodai K, Kodama M (2001) J Electrochem Soc 148:A67
23. Nan J, Hou X, Yang M, Han D, Li W (2006) J Electrochem Soc 153:A1159
24. Yuan AB, Cheng SO, Zhang JQ, Cao CN (1998) J Power Sources 76:36
25. He XM, Ren JG, Li W, Jiang CY, Wan CR (2006) Electrochim Acta 51:4533
26. Zhang X, Gong Z, Zhao S, Geng M, Wang Y, Northwood DO (2008) J Power Sources 175:630
27. Begum SN, Muralidharan VS, Ahmed Basha C (2009) Int J Hydrogen Energy 34:1548
28. Kibria MF, Mridha MS (1996) Int J Hydrogen Energy 21:179
29. Unates ME, Folquer ME, Vilche JR, Arvia AJ (1992) J Electrochem Soc 139:2697
30. Maeda A, Kimiya H, Moriwaki Y, Matsumoto I, Maita A, Kimiya K (1999) EP923146A1
31. Liu B, Yuan H, Zhang Y (2004) Int J Hydrogen Energy 29:453
32. Zhao YL, Wang JM, Chen H, Pan T, Zhang JQ, Cao CN (2004) Electrochim Acta 50:91
33. Brug GJ, van den Eeden ALG, Sluyters-Rehbach M, Sluyters JH (1984) J Electroanal Chem 176:275
34. Rammelt U, Reinhard G (1990) Electrochimica Acta 35:1045
35. Viswanathan VV, Salkind AJ, Kelley JJ, Ockerman JB (1995) J Appl Electrochem 25:716
36. Reid MA, Loyselle PL (1991) J Power Sources 36:285
37. Wang XY, Yan J, Yuan HT, Zhang YS, Song DY (1999) Int J Hydrogen Energy 24:973